Braz J Phys (2014) 44:39–44
DOI 10.1007/s13538-013-0155-9

SOCIEDADE BRASILEIRA DE FÍSICA

CONDENSED MATTER

# Transformation Process of the Magnetron-Sputtered $Ag_2O$ Film in Hydrogen Annealing

**Xiao-Yong Gao · Meng-Ke Zhao · Hong-Tao Liu · Sa Zhang**

Received: 6 April 2013 / Published online: 29 August 2013


**Abstract** The current paper addresses the effect of the hydrogen partial pressure on the microstructure and transformation of the $Ag_2O$ film. The transformation process and mechanism were also analyzed in detail. Increasing the hydrogen partial pressure can accelerate the transformation of $Ag_2O$ to Ag and lower the critical transformation temperature of the film due to the enhanced hydrogen reduction and to both of the lowered activation energy of the reaction of $Ag_2O$ with hydrogen and enhanced lattice strain of the $Ag_2O$ film. The hydrogen-involved reaction in the whole hydrogen annealing process is mainly hydrogen reduction reaction with $Ag_2O$. Diffusion of hydrogen and gaseous $H_2O$ molecules accompanies the whole hydrogen annealing process.

**Keywords** $Ag_2O$ film · Hydrogen annealing · Hydrogen partial pressure · Transformation mechanism

**Mathematics Subject Classifications (2010)** 74E15 · 74F05 · 74N15 · 74A50

## 1 Introduction

$Ag_xO$ films have attracted considerable attention because of their potential application in optical and magneto-optical storage. In 1992, Tominaga et al. [1] first reported that $Ag_xO$ films can be used as substitutes for the organic material commonly used as the storage material in recordable compact discs. Chiu et al. [2] and Kim et al. [3] suggested that $Ag_xO$ can be used as a mask layer in a magneto-optical disc to produce a high-resolution aperture and enhance the magneto-optical signals. In 2003, Zhang et al. [4] discovered the dynamically activated luminescence emission of $Ag_xO$ films, proving that $Ag_xO$ films can be used as nanoscale optical storage materials. According to previous reports, $Ag_xO$ contains several phases, namely, AgO, $Ag_2O$, $Ag_3O_4$ [5], $Ag_4O_3$ [6], and $Ag_2O_3$, of which $Ag_2O$ is the most thermodynamically stable. The magnetron-sputtered $Ag_xO$ film is usually biphased (including AgO and $Ag_2O$ phases). However, the use of the $Ag_xO$ film as a new-generation disc material depends on whether it can be used as an optical switch. In 2006, an experiment was performed by Qin et al. [7] to study the ablation of the $Ag_xO$ film under different laser powers. The results suggested that the $Ag_xO$ film can be used as an optical and magneto-optical storage material mainly because of its thermal decomposition reaction. Chuang et al. [8] pointed out that the critical thermal decomposition temperature (CDT) of the AgO and $Ag_2O$ phases are 160 and 380 °C, respectively, whereas Abe et al. [9] found that the CDT of the $Ag_2O$ film deposited via radio-frequency magnetron reactive sputtering is between 200 and 400 °C. Gao et al. [10] previously reported that the $Ag_xO$ film deposited via direct-current magnetron reactive sputtering (DC sputtering) consists of AgO and $Ag_2O$ phases, with CDTs at 200 and 300 °C, respectively. As recently reported by Gao et al. [11], a <111> preferentially oriented $Ag_2O$ film is deposited on a glass substrate via DC sputtering. The $Ag_2O$ film was then annealed using an optical excitation-assisted rapid thermal annealing under a nitrogen protection condition [12] and a traditional chamber annealing under a

X.-Y. Gao (✉) · M.-K. Zhao · H.-T. Liu · S. Zhang
Key Laboratory of Material Physics of Ministry of Education, School of Physics and Engineering, Zhengzhou University, Zhengzhou 450052, China
e-mail: xygao@zzu.edu.cn

vacuum condition [13] to determine its thermal stability. In the annealing process, $Ag_2O$ begins to transform into Ag and $O_2$ at a CDT of approximately 200 °C. In addition, $O_2$ diffusion is accompanied by the thermal decomposition of $Ag_2O$.

Hydrogen annealing may play different roles in different films. Liu et al. [14] reported that the electrical property and crystal quality of ZnO films significantly changed after hydrogen annealing. Han et al. [15] reported that hydrogen atoms interstitially couple to oxygen and form hydroxyl $(HO)^-$ ions, resulting in the loss of oxygen during the hydrogen annealing of the $Ti_{0.93}O_3$ film. Gao et al. [16] reported that the hydrogen reduction effect can lower the critical transformation temperature (CTT) of $Ag_2O$ to 175 °C at a hydrogen partial pressure (HPP = $[H_2]$/([Ar]+$[H_2]$)) of 25 %. However, no systematic investigation on the effect of HPP on the microstructure and transformation of the hydrogen-annealed $Ag_2O$ films has been conducted. In addition, using hydrogen annealing is effective to obtain the information on the transformation process and mechanism of $Ag_2O$. Hence, the current paper focuses on the effect of HPP on the microstructure and transformation of the $Ag_2O$ film and the roles that hydrogen plays in hydrogen annealing to obtain deeper insight into the transformation process and mechanism of the $Ag_2O$ film.

## 2 Experiment

A single-phase, <111>-oriented $Ag_2O$ film was first deposited on glass substrates via DC magnetron sputtering at a working pressure of 2.5 Pa, a substrate temperature of 250 °C, and an $O_2$-to-Ar flow ratio of 15:18. A high-purity (99.995 %) silver plate was used as the sputtering target. During film deposition, the sputtering power was maintained at 95 W and the electrode distance at 35 mm. Prior to film preparation, the glass substrate was rinsed sequentially with acetone and alcohol in an ultrasonic bath for 15 min, and then placed in an ultrahigh vacuum chamber previously evacuated to a base pressure below $1\times10^{-4}$ Pa. The thickness of the as-deposited $Ag_2O$ film is approximately 920 nm. The Ag target was first pre-sputtered for 5 min before the preparation of $Ag_2O$ film. The gas flow ratio of oxygen to argon was accurately controlled by a mass flow controller. The injected oxygen and Ar were first mixed in a mixer and then injected to the chamber. In addition, the substrate temperature and working pressure were controlled using a thermal coupler and a high-precision vacuum meter, respectively. The as-deposited $Ag_2O$ film was then annealed for 1 h at different HPPs using different hydrogen annealing temperatures ($T_a$). The chosen HPP values in the hydrogen annealing are 10, 20, 30, 40, and 50 %. The working pressure during hydrogen annealing was maintained at 133 Pa. Afterwards, the films were naturally cooled to room temperature.

The crystalline structure of the film was measured using an X-ray diffractometer (Philips PANalytical X'pert) with a $CuK_\alpha$ ($\lambda$= 0.1540598 nm) as the radiation source. The surface morphology was determined using a cold-field scanning electron microscope (JSM-6700F). All measurements were conducted at room temperature.

## 3 Results and Discussion

Figure 1 shows the X-ray diffraction patterns of the $Ag_2O$ film hydrogen annealed at different $T_a$ values and at an HPP of 10 %. Wei et al. [17] pointed out that the electrodeposited silver oxide nanostructures have a defective cubic structure containing also amorphous zones. However, no defective cubic structure containing any amorphous zones for the magnetron-sputtered $Ag_2O$ film is observed. The $Ag_2O$ (111) diffraction peak is obviously weakened at $T_a$ = 160 °C, and no Ag diffraction peak is discernible. Two weak Ag (111) and (200) diffraction peaks begin to appear at $T_a$ = 175 °C, indicating that $Ag_2O$ begins to transform into Ag at this temperature at an HPP of 10 %. Zhang et al. [13] previously reported that under a vacuum condition, the $Ag_2O$ film begins to thermally decompose into Ag nanoparticles at $T_a$ = 300 °C via chamber annealing, indicating that hydrogen annealing can lower the CTT of the $Ag_2O$ film. Ag diffraction peaks, rather than $Ag_2O$ diffraction peaks, are discerned at $T_a$ = 225 °C.

Figure 2 shows the X-ray diffraction patterns of the $Ag_2O$ film hydrogen annealed at different $T_a$ values using an HPP

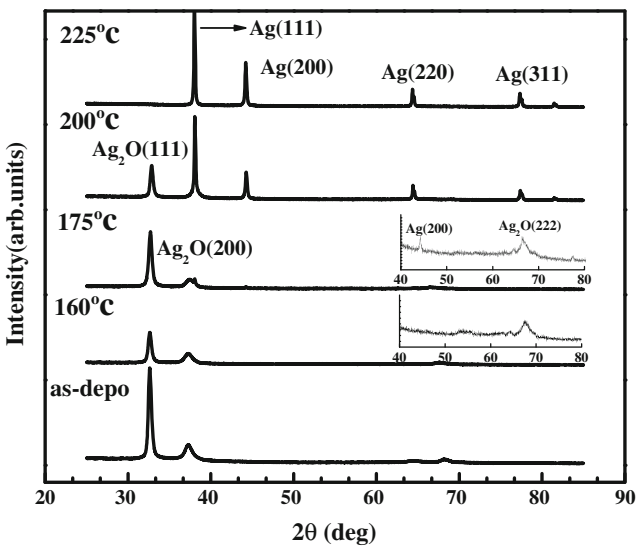


**Fig. 1** X-ray diffraction patterns of the $Ag_2O$ film hydrogen annealed at different $T_a$ values using an HPP of 10 %. The *two insets* display the X-ray diffraction patterns in the $2\theta$ range from 40° to 80°

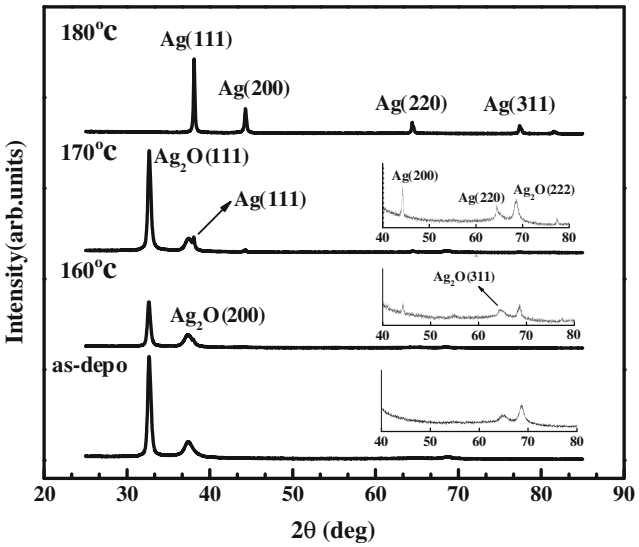


**Fig. 2** X-ray diffraction patterns of the $Ag_2O$ film hydrogen annealed at different $T_a$ values using an HPP of 20 %. The *three insets* display the X-ray diffraction patterns in the $2\theta$ range from 40° to 80°

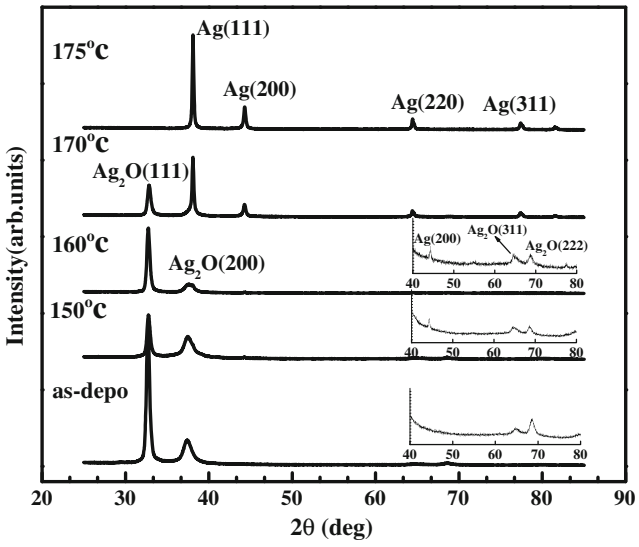


**Fig. 4** X-ray diffraction patterns of the $Ag_2O$ film hydrogen annealed at different $T_a$ values using an HPP of 40 %. The *three insets* display the X-ray diffraction patterns in the $2\theta$ range from 40° to 80°

of 20 %. A similar evolution from $Ag_2O$ to a biphased $Ag_2O$ and Ag complex and to Ag occurs as $T_a$ increases. However, a weak Ag (200) diffraction peak begins to appear at $T_a$ =160 °C. Meanwhile, only Ag diffraction peaks are discerned when $T_a$ is increased to 180 °C. Figure 3 shows the X-ray diffraction patterns of the hydrogen-annealed $Ag_2O$ film using an HPP of 30 %. A very weak but clear Ag (200) diffraction peak begins to appear at $T_a$ =150 °C and becomes strong at $T_a$ = 160 °C, at which the $Ag_2O$ diffraction peak is obviously weakened. The $Ag_2O$ diffraction peaks completely disappear at $T_a$ = 175 °C. According to the X-ray diffraction results in Figs. 1, 2, and 3, the CTT of the $Ag_2O$ film is reduced from 175 to 150 °C as the HPP increases from 10 to 30 %, indicating that increasing the HPP can lower down the CTT of the $Ag_2O$ film. The lowered CTT value with increasing HPP is inherently attributed to the lowered activation energy of the reaction of $Ag_2O$ with hydrogen [18]. In fact, this is a consequence of a great drop in free energy of the reaction system caused by the formation of water [18]. To confirm this result, the $Ag_2O$ film was hydrogen annealed using an HPP of 40 and 50 %. The X-ray diffraction patterns of the $Ag_2O$

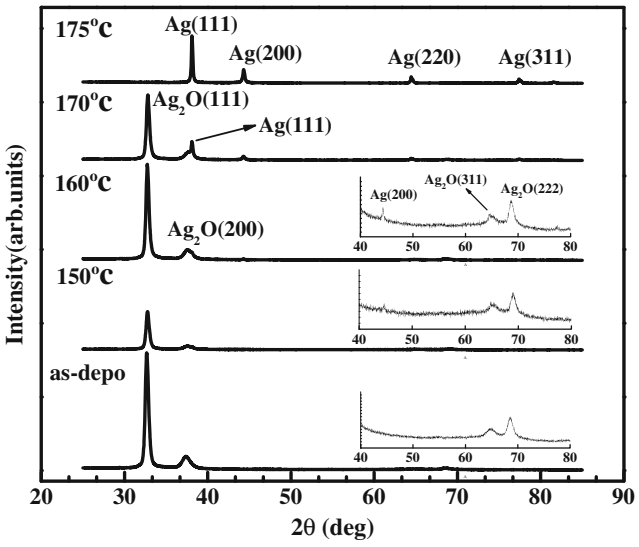


**Fig. 3** X-ray diffraction patterns of the $Ag_2O$ film hydrogen annealed at different $T_a$ values using an HPP of 30 %. The *three insets* display the X-ray diffraction patterns in the $2\theta$ range from 40° to 80°

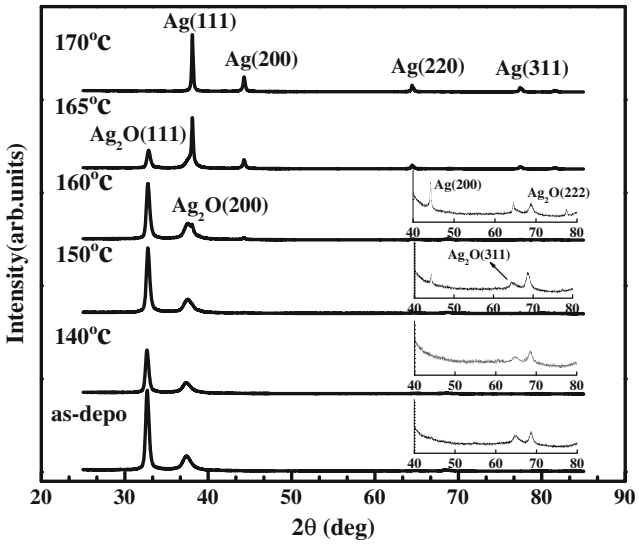


**Fig. 5** X-ray diffraction patterns of the $Ag_2O$ film hydrogen annealed at different $T_a$ values using an HPP of 50 %. The *four insets* display the X-ray diffraction patterns in the $2\theta$ range from 40° to 80°

films are shown in Figs. 4 and 5, respectively. A weak Ag (200) diffraction peak begins to appears at $T_a = 150$ °C (Fig. 4), accompanied by a weakened $Ag_2O$ diffraction peak. The Ag diffraction peaks become much stronger than the $Ag_2O$ diffraction peaks at $T_a = 170$ °C, and only Ag diffraction peaks are discernible at $T_a = 175$ °C. Figure 5 shows the appearance of the Ag (200) diffraction peak at $T_a = 150$ °C, whereas no Ag diffraction peak appears at $T_a = 140$ °C. Notably, only Ag diffraction peaks are discernible at $T_a = 170$ °C. The X-ray diffraction results in Figs. 4 and 5 indicate that the CTT of the $Ag_2O$ film is maintained at 150 °C as the HPP exceeds 30 %. Compared with the results in Figs. 1 to 3, increasing the HPP can accelerate the transformation of $Ag_2O$ to Ag, which is attributed to the reduction role that hydrogen plays in the hydrogen annealing of the $Ag_2O$ film.

Two effects may coexist during the hydrogen annealing process. One is the thermal decomposition of the film because of the thermal effect and the other one is film reduction due to the hydrogen reduction effect. However, the former occurs only at $T_a \geq 200$ °C [16] in the absence of hydrogen. The former may not occur in parallel to the reduction reaction due to the slow thermal decomposition. On the other hand, the enthalpy of adsorption of H atoms on $Ag_2O$ surface exceeds the enthalpy of dissociation of $H_2$ molecule. Adsorption of $H_2$ molecules cannot provide enough energy to proceed the dissociation of $H_2$ molecule on $Ag_2O$ surface [19]. Thereafter, the hydrogen reduction effect involved in the entire hydrogen annealing process is described as follows:

$$Ag_2O + H_2(g) = 2Ag(s) + H_2O(g) \quad (1)$$

When HPP is increased, more $H_2$ molecules may be adsorbed on the $Ag_2O$ film surface to accelerate the transformation of $Ag_2O$ to Ag, causing the reduction in the CTT. However, the concentration of the $H_2$ molecules adsorbed on the film surface may increase to saturation when HPP exceeds 30 %. The transformation of $Ag_2O$ to Ag will no longer be accelerated, causing the CTT to remain unchanged even when HPP further increases.

The decrease in the CTT of $Ag_2O$ may also be attributed to the enhanced lattice distortion of the film besides being due to the lowered activation energy of the reaction of film with hydrogen. Table 1 presents the average grain size and lattice strain of the $Ag_2O$ film, as calculated in accordance with Williamson–Hall relation [20, 21]:

$$\beta \cos\theta = \lambda/D + 4 \times \Delta d/d \times \sin\theta \quad (2)$$

$$\beta^2 = {\beta_M}^2 - {\beta_S}^2, \quad (3)$$

where $\lambda$, $\theta$, $D$, $d$, and $\Delta d/d$ are the X-ray wavelength, diffraction angle, average grain size, interplanar spacing, and lattice strain, respectively, $\beta$ is the full width at half maximum (FWHM) caused by the grain size and the lattice strain, and $\beta_M$ and $\beta_S$ are the measured FWHM of film and standard FWHM of the guide sample, respectively. The $D$ and $\Delta d/d$ can be obtained by the linear fitting of $\beta \cos\theta$ vs $\sin\theta$ for all the diffraction peaks in accordance with Williamson–Hall relation, which can be automatically conducted by the software (X'Pert HighScore Plus) accompanied with the XRD instrument (Philips PANAlytical X'Pert). The results indicate that a smaller average grain size leads to a larger lattice strain because of the enhanced grain surface effect. The lattice distortion is characterized by the gradually increasing lattice strain with increasing $T_a$ at different HPPs, resulting in a less compact film surface. In this case, the $H_2$ molecules adsorbed on the $Ag_2O$ film surface may easily diffuse into the loose film and lead to an accelerated transformation of $Ag_2O$. To confirm this conclusion, the surface morphology of the $Ag_2O$ film hydrogen annealed at different $T_a$ values using an HPP of 10 % was measured using a cold-field scanning electron microscope (Fig. 6). To obtain clear SEM images, carbon was sprayed on the surface of $Ag_2O$ film to enhance the surface conductivity. The $Ag_2O$ film hydrogen annealed at $T_a = 150$ °C shows a compact and uniform surface similar to the surface structure of the as-deposited $Ag_2O$ film. However, the $Ag_2O$ film hydrogen-annealed at $T_a = 175$ °C demonstrates a loose structure, and some holes begin to appear. According to Fig. 1, $Ag_2O$ begins to transform into Ag at $T_a = 175$ °C at an HPP of 10 %. The $H_2$ molecules adsorbed on the $Ag_2O$ film surface may diffuse through the holes and accelerate the transformation of $Ag_2O$ to Ag via the hydrogen reduction effect. Gaseous $H_2O$ molecules may also diffuse to the film surface through these holes. After hydrogen annealing at 200 and 225 °C, the $Ag_2O$ film surface becomes much looser and more porous,

**Table 1** Calculated average grain size and lattice strain of the $Ag_2O$ film

| HPP (%) | $T_a$ (°C) | Grain size (nm) | Lattice strain (%) |
|---|---|---|---|
| 20 | As-depo | 61.8 | 0.315 |
| 20 | 160 | 54.8 | 0.344 |
| 20 | 170 | 45.0 | 0.395 |
| 30 | As-depo | 38.0 | 0.450 |
| 30 | 150 | 35.2 | 0.476 |
| 30 | 160 | 32.9 | 0.500 |
| 40 | As-depo | 38.0 | 0.448 |
| 40 | 150 | 38.0 | 0.449 |
| 40 | 160 | 30.9 | 0.526 |
| 50 | As-depo | 54.8 | 0.343 |
| 50 | 140 | 45.0 | 0.394 |
| 50 | 150 | 45.0 | 0.395 |
| 50 | 160 | 41.2 | 0.421 |

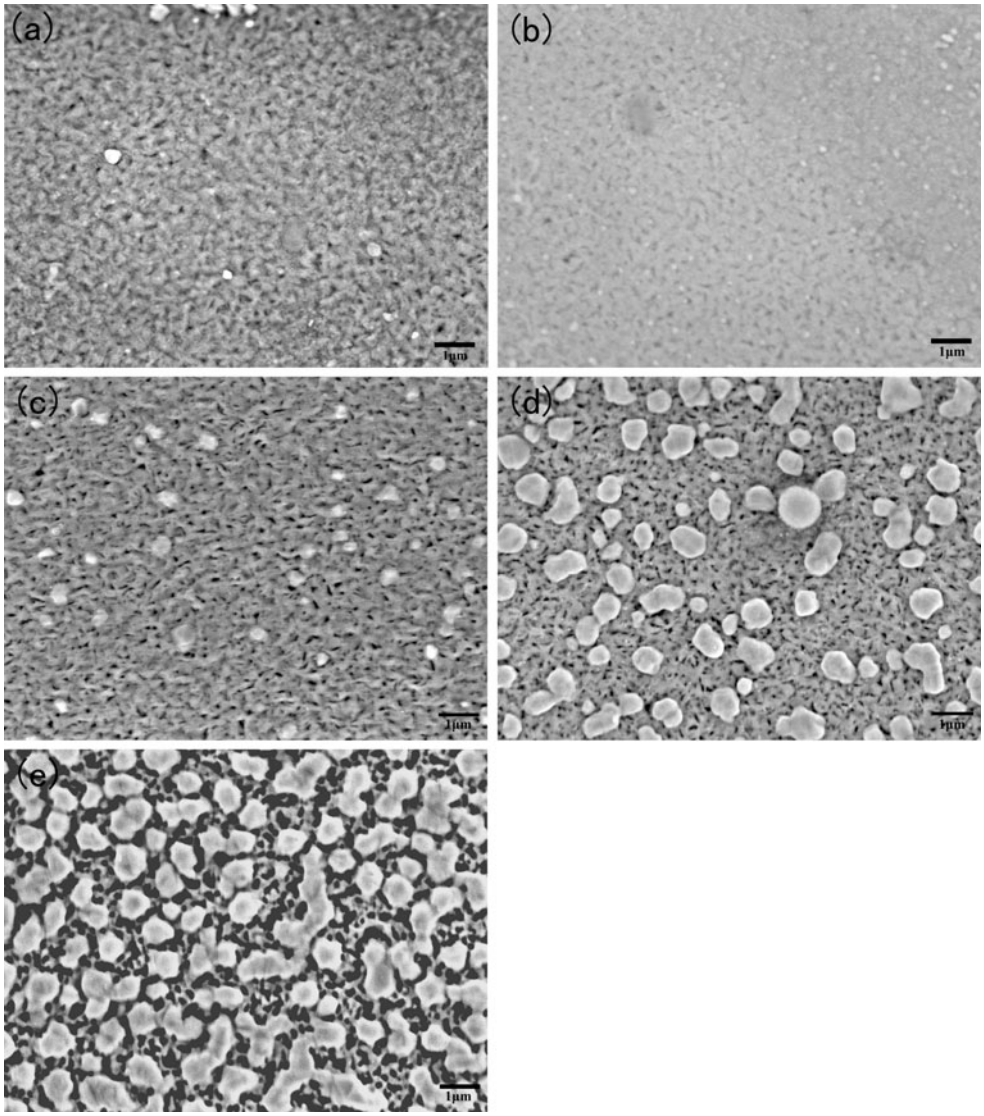


**Fig. 6** Surface morphology of the $Ag_2O$ films hydrogen annealed at temperature of (**a**) as-depo, (**b**) 160 °C, (**c**) 175 °C, (**d**) 200 °C, and (**e**) 225 °C

again resulting in the accelerated transformation of $Ag_2O$ to Ag via the hydrogen reduction effect. More gaseous $H_2O$ molecules arising from the hydrogen reduction of the $Ag_2O$ film may also diffuse to the film surface through these holes. Hence, increasing the $T_a$ and HPP may accelerate the transformation of the $Ag_2O$ film. Increasing the HPP up to 30 % may lower the CTT of the $Ag_2O$ film inherently because of the lowered activation energy of the reaction of $Ag_2O$ with hydrogen and the enhanced lattice strain of $Ag_2O$ film. It is worthy to be noted that in subpanels a and c–e of Fig. 6, some agglomerates are discernible whereas none of them appears in Fig. 6b. The surface particle agglomerates may be due to a combination of different effects including not only the transformation of the film but also distortion of the SEM image at the pores. The inherent mechanism is still to be further studied.

## 4 Conclusions

$Ag_2O$ films preferentially <111> oriented were deposited on glass substrates via DC magnetron sputtering and then annealed at different temperatures using different HPPs. The main results are as follows:

1. Increasing the HPP and $T_a$ can accelerate the transformation of the $Ag_2O$ film because of the enhanced hydrogen reduction and the enhanced lattice distortion;
2. Increasing the HPP (HPP $\leq$ 30 %) can lower the CTT of the $Ag_2O$, which is inherently attributed to both the lowered activation energy of the reaction of $Ag_2O$ with hydrogen and the enhanced lattice strain of $Ag_2O$ film. When the HPP surpass 30 %, the CTT will remain unchanged even when HPP further increases.

3. Hydrogen mainly acts as the reducing agent in the hydrogen annealing of the $Ag_2O$ film. The hydrogen-involved reaction in the whole hydrogen annealing process is mainly hydrogen reduction reaction with $Ag_2O$. In addition, diffusion of hydrogen and gaseous $H_2O$ molecules accompanies the whole hydrogen annealing process.

**Acknowledgments** The authors are grateful for the supports from the National Natural Science Foundation of China (grant no. 60807001), the Foundation of Young Key Teachers from University of Henan Province (grant no. 2011GGJS-008), the Foundation of Graduate Education Support of Zhengzhou University, the Foundation of Graduate Innovation of Zhengzhou University (grant no. 12L00104), and the Foundation of Henan Educational Committee (grant no. 2010A140017).

## References

1. J. Tominaga, T. Nakano, N. Atoda, in *Extended Abstracts of the 39th Spring Meeting of the Japan Society of Applied Physics and Related Societies, 30 aL-3*. (Nippon Univ., Narashino, 1993)
2. Y. Chiu, U. Rambabu, M.H. Hsu, H.P.D. Shieh, C.Y. Chen, H.H. Lin, J. Appl. Phys. **94**, 1996 (2003)
3. J. Kim, H. Fuji, Y. Yamakama, T. Nakano, D. Büchel, J. Tominaga, N. Atoda, Jpn. J. Appl. Phys. **40**, 1634 (2001)
4. X.Y. Zhang, X.Y. Pan, Q.F. Zhang, B.X. Xu, H.B. Jiang, C.L. Liu, Q.H. Gong, J.H. Wu, Acta Phys.-Chim. Sin. **19**, 203 (2003). (in Chinese)
5. B. Standke, M. Jansen, Angew. Chem. Int. Ed. **25**, 77 (1986)
6. A.N. Mansour, J. Phys. Chem. **94**, 1006 (1990)
7. L.J. Qin, Z. Wang, Y.G. Jia, H.Z. Xu, G.D. Wang, J. Funct. Mater. **1**(37), 139 (2006)
8. H.J. Chuang, H.W. Ko, Proc. Natl. Sci. Counc. ROC. A **13**, 145 (1989)
9. Y. Abe, T. Hasegawa, M. Kawamura, K. Sasaki, Vacuum **76**, 1 (2004)
10. X.Y. Gao, S.Y. Wang, J. Li, Y.X. Zheng, R.J. Zhang, P. Zhou, Y.M. Yang, L.Y. Chen, Thin Solid Films. **455–456**, 438 (2004)
11. X.Y. Gao, H.L. Feng, J.M. Ma, Z.Y. Zhang, J.X. Lu, Y.S. Chen, S.E. Yang, J.H. Gu, Phys. B. **405**, 1922 (2010)
12. X.Y. Gao, H.L. Feng, Z.Y. Zhang, J.M. Ma, J.X. Lu, China Phys. Lett. **27**, 026804 (2010)
13. Z.Y. Zhang, X.Y. Gao, H.L. Feng, J.M. Ma, J.X. Lu, Acta Phys. Sin. **60**, 036107 (2011). (in Chinese)
14. W.W. Liu, B. Yao, Y.F. Li, B.H. Li, C.J. Zheng, B.Y. Zhang, C.X. Shan, Z.Z. Zhang, J.Y. Zhang, D.Z. Shen, Appl. Surf. Sci. **255**, 6745 (2009)
15. K.B. Han, C.S. Kim, C.H. Jeon, H.S. Jhon, S.Y. Lee, Mat. Sci. Eng. B-Solid. **109**, 170 (2004)
16. X.Y. Gao, M.K. Zhao, Z.Y. Zhang, C. Chen, J.M. Ma, J.X. Lu, Thin Solid Films **519**, 6620 (2011)
17. W.F. Wei, X.H. Mao, L.A. Ortiz, D.R. Sadoway, J. Mater. Chem. **21**, 432 (2011)
18. D. Jelić, J. Penavin-Ŝkundrić, D. Majstorović, S. Mentus, Thermochim. Acta. **526**, 252 (2011)
19. D. Vasic, Z. Ristanovic, I. Pasti, S. Mentus, Russ. J. Phys. Chem. A. **85**, 2373 (2011)
20. X.C. Mi, Y.Y. Chen, Z.J. Wu, X.H. Liu, S.Y. Yang, L.C. Zhang, PARTA Phys. Test. **40**(4), 179 (2004). (in Chinese)
21. X.Y. Fan, S.M. Ma, China Ceram. Ind. **9**(1), 43 (2002). (in Chinese)